OMICS Journal of Radiology
ISSN: 2167-7964

Kawamorita et al., OMICS J Radiol 2015, 4:4
DOI: 10.4172/2167-7964.1000202

Research Article Open Access

Novel Anisotropic Margin Calculation Based On the Cumulative Frequency Distribution of Uncertainties in the Clinical Target Volume

Ryu Kawamorita[1,2*], Hajime Monzen[1], Wataru Okada[2], Ryuta Nakahara[2], Shun Kishimoto[2], Kentaro Ishii[2], Toshifumi Nakajima[2] and Yasumasa Nishimura[1]

[1]*Department of Radiation Oncology, Kinki University, Faculty of Medicine, Osaka-Sayama, Osaka, Japan*
[2]*Department of Radiation Oncology, Tane General Hospital, Osaka-Nishiku, Osaka, Japan.*

Abstract

Objective: The purpose of this study was to determine the PTV margins from the cumulative frequency of uncertainties of the clinical target volume (CTV) position obtained using hybrid-image guided radiotherapy (H-IGRT) with volumetric-modulated arc therapy (VMAT).

Materials and Methods: Study participants were 22 patients with intermediate-risk prostate cancer who underwent VMAT. All patients were treated using the following image-guided (IG) procedure: 1) no-correction skin mark setup (no-IG); 2) bony anatomy registration with 2D-imaging (2D-IG); and 3) organ registration using CBCT images (3D-IG). The systematic (Σ_{tot}) and random (σ_{tot}) errors were obtained from the no-IG, 2D-IG, and 3D-IG registration images of 198 fractions. The PTV margin was computed using the cumulative frequency distribution of the actual position errors of the CTV, and which was compared with the formulation by MPTV = 2.5 Σ_{tot} + 0.7 σ_{tot}.

Results: The margin size of 3D IG procedure was as follows: 3D-IG: 7.6, 5.4, and 3.5 mm for the AP, SI, and LR axes, respectively. Using M_{PTV} = 2.5 Σ_{tot} + 0.7 σ_{tot}: 3D-IG: 4.2, 3.7, and 1.3 mm for the AP, SI, and LR axes, respectively. In M_{PTV}: = α Σ_{tot} + β σ_{tot}, the coefficients α and β were α = 3.4, 2.3, and 4.6 and β = 2.9, 3.0, and 3.0 for AP, SI, and LR, respectively.

Conclusion: The margin size (M_{PTV}) calculated by our modified formulation based on the margin direction satisfied 99% of the prescription dose coverage in each direction and a minimum of 95% of the dose coverage to the CTV for all patients using H-IGRT.

Keywords: Hybrid image-guided radiotherapy; Planning target volume margin; Prostate cancer; CTV position uncertainty

Introduction

Online image guided radiotherapy (IGRT) is used for prostate registration for prostate cancer patients [1-5]. At our hospital, online correction via a three-step setup protocol with hybrid-image guided radiotherapy (H-IGRT) is conducted, i.e., two-dimensional (2D)/three-dimensional (3D) and 3D/3D registrations are performed using H-IGRT. Our IGRT protocol preferentially uses organ registration relative to the anterior rectal wall, which corrects for almost all systematic errors; however, several random errors remain. Setup correction protocols may reduce geometric treatment uncertainties and the clinical target volume (CTV)-to-planning target volume (PTV) margins. Therefore, a novel approach is required for PTV margin calculations (M_{PTV}) in H-IGRT that accounts for small systematic uncertainty, random uncertainty and target registration residual error (TRE) depend on H-IGRT system, in contrast to the more general formulation by van Herk et al., i.e., M_{PTV} = 2.5 Σ + 0.7 σ, which accounts for the population systematic uncertainty Σ and random uncertainty σ. This formula (M_{PTV} = 2.5 Σ + 0.7 σ) was computed with statistical procedure using systematic and random uncertainties of CTV position [6]. Furthermore, the coefficients of the model parameters were numerically calculated under a spherically symmetric condition thereby leading to an isotropic margin perpendicular to a spherical tumor surface. However, did not consider about residual error to be TRE in case of using IGRT. For example, as TRE arise due to deformation of prostate and/or seminal vesicles even if the registration at CTV using image guidance with CBCT. The purpose of this study was to determine the PTV margins from the cumulative frequency of CTV uncertainties include TRE obtained by an H-IGRT system.

Materials and Methods

Patients and treatment plan

Twenty-two intermediate-risk prostate cancer patients who were treated using VMAT between 2012 and 2013 were included in this study. All patients were immobilized in a position using a vacuum cushion (Vac-Lok; MedTech, Orange City, IA, USA). Computed tomography (CT) scans were acquired with 2.5 mm slice thicknesses using a 16–detector row CT scanner (Optima CT580W; GE Medical Systems, Waukesha, WI, USA) from the lower abdomen to 50.0 mm below the ischial tuberosity. The initial reference markers and associated skin marks were placed at the time of CT simulation.

CTV was defined as the entire prostate and the proximal 15.0 mm of the seminal vesicles. PTV was generated by adding an 8.0 mm margin to CTV in all dimensions except posteriorly, where a 5.0 mm margin was used. Contouring of the organ at risk (OAR) included the rectum, bladder, femoral heads, penile bulb, and small bowel, defined according to the Radiation Therapy Oncology Group (RTOG) pelvic

***Corresponding author:** Ryu Kawamorita, Department of Radiation Oncology, Tane General Hospital, 1-12-21, Kujo-Minami, Nishi-ku, Osaka city, Osaka 550-0025, Japan, Tel: +81-6-6581-1071; Fax: +81-6-6585-2772; E-mail: kawamorita@tane.or.jp

Received July 18, 2014; **Accepted** August 11, 2015; **Published** August 14, 2015

Citation: Kawamorita R, Monzen H, Okada W, Nakahara R, Kishimoto S, et al. (2015) Novel Anisotropic Margin Calculation Based On the Cumulative Frequency Distribution of Uncertainties in the Clinical Target Volume. OMICS J Radiol 4: 202. doi:10.4172/2167-7964.1000202

normal tissue contouring guidelines [7]. The total prescription dose was 78.0 Gy to the PTV at 2.0 Gy per fraction. Dose normalization was set to the PTV mean dose. The treatment plans were generated using single-arc VMAT (358 degree; 74 sec per rotation). All treatment plans were developed using Eclipse™ ver.10.0 planning software (Varian Medical Systems, Palo Alto, CA, USA) for 10 MV photon irradiation. The dose was calculated using the Analytical Anisotropic Algorithm in Eclipse™.

To verify leaf motion of each beam or specific patient's plans, various quality assurance tests were conducted [8,9]. Once the VMAT plan was developed and approved, CT simulation datasets were imported into the ExacTrac® X-ray 6D system (BrainLab AG, Feldkirchen, Germany) for 2D/3D registration using digital reconstructed radiographs (DRRs) of 2D oblique images to the planning CT images [10]. The CT simulation datasets were also imported into the ARIA record and verification system (Varian Medical Systems, Palo Alto, CA, USA) for 3D/3D registration using CBCT images and planning CT images [11,12]. VMAT was delivered using linear accelerators equipped with a high-definition multi-leaf collimator (HD-MLC; spatial resolution: 2.5 mm at the isocenter; Novalis TX; BrainLab AG, Feldkirchen, Germany). The daily treatment time, including image registration from the final image acquisition until the end of irradiation, was 4 to 6 min. Before each fractionation, the bladder and rectum volume were prepared in the same way as at the time of CT simulation.

IGRT strategy for prostate cancer at our hospital

Figure 1 shows a diagram of the IGRT procedure used in this study. The H-IGRT system consisted of an ExacTrac® X-ray 6D system and linear accelerator equipped with CBCT. All patients were treated using the step-by-step IG procedures involving no-correction skin mark setup (no image guidance; no-IG), bony anatomy 3D registration using 2D images from ExacTrac® X-ray 6D system (2D image guidance; 2D-IG), and 3D organ registration using CBCT images (3D image guidance; 3D-IG).

Firstly, the no-IG procedure was used to align the skin mark with the lasers. However, setup residual error of the CTV arose due to geometrical constraints associated with the bony anatomy [11,13]. Also, a systematic pitching error (maximum: 2.0 mm) was present due to the difference between the flexibility of the CT couch and that of

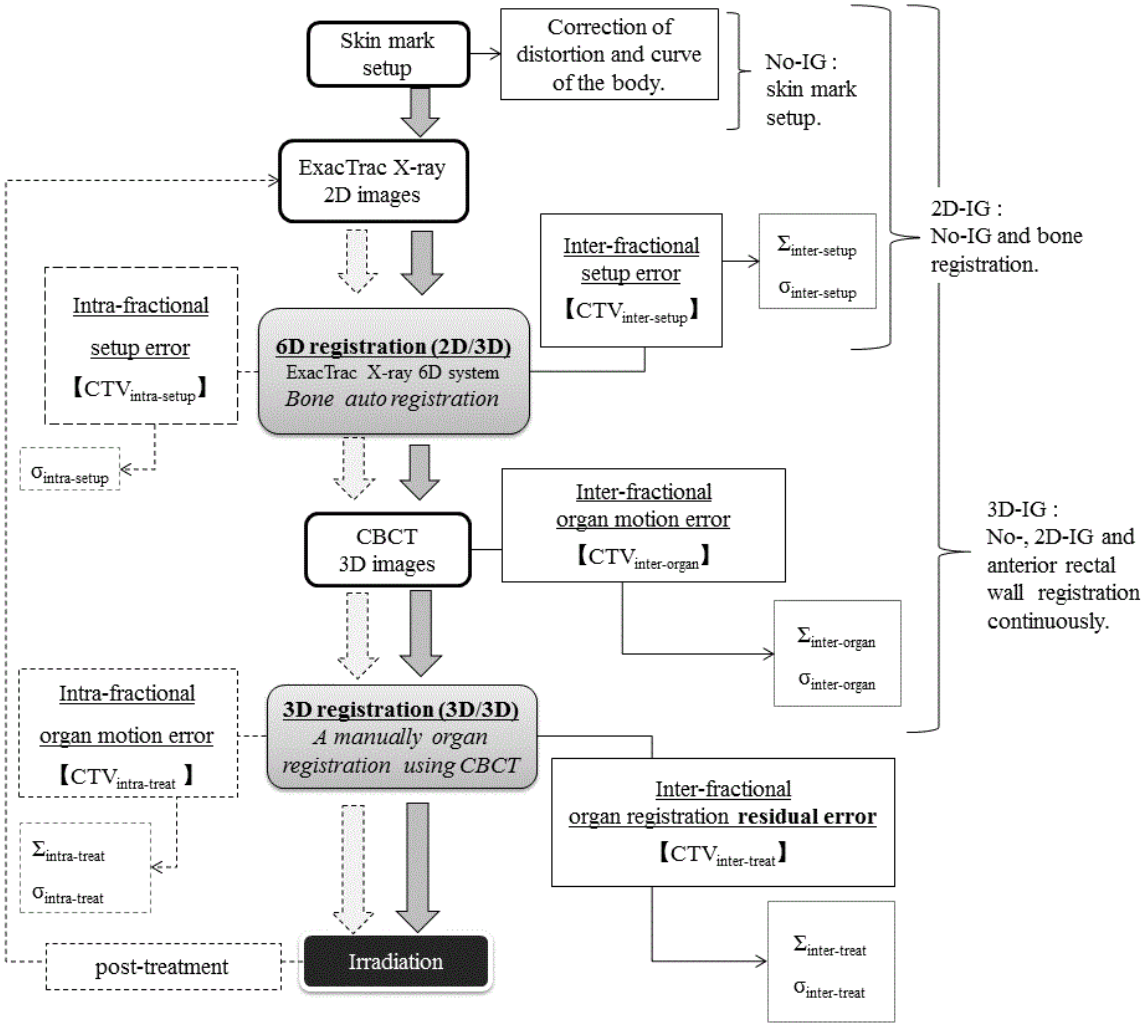

Figure 1: Hybrid image-guided radiotherapy (H-IGRT) strategy used in our institute. The solid arrowheads represent the pre-treatment procedure for IGRT error detection, and the dotted arrowheads correspond to the post-treatment procedure for IGRT error detection.

the linear accelerator treatment couch. Therefore, as a next step, the 2D-IG procedure using the ExacTrac® X-ray 6D system was used to correct for the setup residual error of the bony anatomy and systematic pitching error of the linear accelerator treatment couch. At the same time, the inter-fractional setup error was calculated by the BrainLab iterative rigid registration process, which uses mutual information as a similarity measure for its calculation [10,11]. Subsequently, inter-fractional organ motion error was corrected using 3D-IG, with priority given to the anterior rectal wall while simultaneously ensuring that the portion of the rectum overlapping the PTV is excluded.

Uncertainty component of the CTV for each image guidance procedure

Inter- and intra-fractional variations in the CTV positions relative to the treatment beam were represented as systematic (Σ) or random (σ) uncertainties which were calculated based on components of each CTV in the Table 1, respectively. Σ is the standard deviation of the overall means per patient (M), σ is the overall standard deviation of the population, and Σ and σ uncertainties were calculated from 2D- and 3D-IG image set data. The authors evaluated a total of 396 image sets for inter-fractional variation (198 fractions) and a total of 288 image sets for intra-fractional variation (144 fractions) in the CTV position for the 22 patients.

Inter-fractional systematic ($\Sigma_{inter\text{-}setup}$) and random ($\sigma_{inter\text{-}setup}$) setup uncertainties of the bony anatomy were calculated from bony anatomy registration data obtained from 2D-IG images (Figure 1).

The CTV position error associated with our setup was categorized into inter- and intra-fractional bony anatomy error ($CTV_{inter\text{-}setup}$ and $CTV_{intra\text{-}setup}$) [14]. Inter-fractional organ motion systematic ($\Sigma_{inter\text{-}org}$) and random ($\sigma_{inter\text{-}org}$) uncertainties of the CTV were calculated between the planning CTV position and the CTV position after 2D-IG bony anatomy registration, which was obtained by preregistration of the 3D-IG images; these CTV uncertainty components were defined as $CTV_{inter\text{-}organ}$ (Figure 1). Note that $\Sigma_{inter\text{-}org}$ and $\sigma_{inter\text{-}org}$ include the position error due to deformation [15-17]. Although $\Sigma_{inter\text{-}org}$ and $\sigma_{inter\text{-}org}$ were corrected using 3D-IG, inter-fractional residual systematic ($\Sigma_{inter\text{-}treat}$) and random ($\sigma_{inter\text{-}treat}$) uncertainties of the CTV remained due to the anterior rectal wall reference with 3D-IG. Consequently, $\Sigma_{inter\text{-}treat}$ and $\sigma_{inter\text{-}treat}$ were calculated using the difference between the planning CTV position and the final CTV position used for treatment in the hybrid image guidance ($CTV_{inter\text{-}treat}$), i.e., the final CTV position after the no-IG, 2D-IG, and 3D-IG procedures. As described above, 3D-IG was performed with preferential registration given to the anterior rectal wall in this study. Therefore, $CTV_{inter\text{-}treat}$ was included in the deformation error of the CTV due to rectal deformation and/or filling as well as inter-fractional prostate motion error (Figure 2).

The intra-fractional setup random uncertainty ($\sigma_{intra\text{-}setup}$) was calculated from the pre- and post-treatment position error of the bony anatomy. Systematic ($\Sigma_{intra\text{-}treat}$) and random ($\sigma_{intra\text{-}treat}$) uncertainties for intra-fractional organ motion were calculated from the position error during the $CTV_{inter\text{-}treat}$ fraction ($CTV_{intra\text{-}treat}$). $\sigma_{intra\text{-}setup}$, $\Sigma_{intra\text{-}treat}$, and $\sigma_{intra\text{-}treat}$ were calculated using image sets of pre- and post-treatment registration of 16 of 22 patients. These intra-fractional uncertainties were obtained using 2D- and 3D-IG images immediately after irradiation.

$CTV_{inter\text{-}setup}$, $CTV_{intra\text{-}setup}$, $CTV_{inter\text{-}organ}$, $CTV_{inter\text{-}treat}$, and $CTV_{intra\text{-}treat}$ (CTV_{all}) included only translational motion errors related to displacement; rotational angle errors were excluded from evaluation in this study. These five uncertainty components (referred to as CTV_{all}) were included in the residual uncertainty from 3D-IG in addition to the CTV uncertainty reported in the International Committee on Radiation Units (ICRU) Report-62 [18]. The coordinates of CTV_{all} centre were obtained using the isocenter automatic setting function for the PTV. To minimize inter-observer variation, the contouring of organs for definition of the centroid coordinates was performed by a single physicist.

Overall systematic (Σ_{tot}) and random (σ_{tot}) uncertainties

The no-IG, 2D-IG, and 3D-IG procedures all had different overall systematic (Σ_{tot}) and random (σ_{tot}) uncertainty components for the CTV, as shown in Table 1. Σ_{tot} and σ_{tot} of each IGRT were calculated using the root-sum-square (RSS) of the components of CTV_{all}, as shown in Table 1. Σ, σ, and the mean of these uncertainty components are listed in Table 2; the values for Σ and σ are represented as Gaussian

No-IGRT	2D-IGRT	3D-IGRT
$CTV_{inter\text{-}setup}$	-	-
$CTV_{inter\text{-}organ}$	$CTV_{inter\text{-}organ}$	$CTV_{inter\text{-}treat}$
$CTV_{intra\text{-}setup}$	$CTV_{intra\text{-}treat}$	$CTV_{intra\text{-}treat}$
$CTV_{intra\text{-}treat}$	$CTV_{intra\text{-}treat}$	$CTV_{intra\text{-}treat}$
Abbreviations: Please refer to Figure 1.		

Table 1: Uncertainty components of the clinical target volume (CTV) variation with respect to the planning target volume (PTV) margin design.

	AP (mm)	SI (mm)	LR (mm)		AP (mm)	SI (mm)	LR (mm)
$M_{inter\text{-}setup}$	-0.3	0.8	1.4	$M_{intra\text{-}setup}$	-0.9	-0.7	0.0
$\Sigma_{inter\text{-}setup}$	2.0	1.2	1.6	$\Sigma_{intra\text{-}setup}$	-	-	-
$\sigma_{inter\text{-}setup}$	0.6	0.3	0.4	$\sigma_{intra\text{-}setup}$	0.7	0.8	0.2
$M_{inter\text{-}org}$	1.6	0.4	0.2	$M_{inter\text{-}treat}$	0.9	-1.0	0.4
$\Sigma_{inter\text{-}org}$	2.1	1.2	0.3	$\Sigma_{inter\text{-}treat}$	1.1	1.2	0.4
$\sigma_{inter\text{-}org}$	0.4	0.3	0.2	$\sigma_{inter\text{-}treat}$	0.5	0.4	0.2
				$M_{intra\text{-}treat}$	0.8	0.3	-0.1
				$\Sigma_{intra\text{-}treat}$	0.8	0.3	0.2
				$\sigma_{intra\text{-}treat}$	0.6	0.3	0.3
Abbreviations: M: the overall mean of the mean patient-specific error across all patients; Σ: systematic uncertainty, overall standard deviation across all patients of the mean patient-specific error; σ: random uncertainty, standard deviation of the patient-specific standard deviation. AP: anterior–posterior direction; SI: superior–inferior direction; LR: left–right direction.							

Table 2: Systematic (Σ) and random (σ) uncertainties of each CTV acquired from 2D- and 3D-IG data using the proposed H-IGRT strategy.

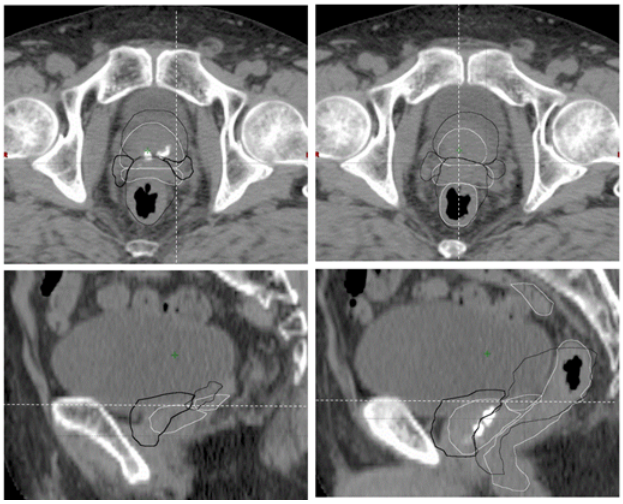

Figure 2: Axial and sagittal images of a slice of the seminal vesicles (left) and central prostate (right). A slice showing large displacement and large deformations owing to rectum filling. Clinical target volume (CTV) of the planning computed tomography (CT) scan (gray) and cone beam CT (CBCT) scan (black) are projected on both data sets. Dashed lines indicate the intersection of the axial and sagittal planes.

distributions.

Equations (1)–(3) were used to calculate Σ_{tot} and σ_{tot} for the PTV margin size for no-IG, 2D-IG, and 3D-IG (no-PTV margin, 2D-PTV margin, and 3D-PTV margin, respectively) [6].

No-PTV margin: skin mark setup correction.

$$\sum_{tot;\,no} = (\sum_{inter-setup}{}^2 + \sum_{inter-org}{}^2 + \sum_{intra-org}{}^2)^{1/2}$$
$$\sigma_{tot;\,no} = (\sigma_{inter-setup}{}^2 + \sigma_{intra-setup}{}^2 + \sigma_{inter-org}{}^2 + \sigma_{intra-org}{}^2)^{1/2} \quad (1)$$

2D-PTV margin: No-IG and bone corrections using 2D-IG.

$$\sum_{tot;2D} = \left(\sum_{inter-org}{}^2 + \sum_{intra-org}{}^2\right)^{1/2}$$
$$\sigma_{tot;2D}\left(\sigma_{intra-setup}{}^2 + \sigma_{inter-org}{}^2 + \sigma_{intra-org}{}^2\right)^{1/2} \quad (2)$$

3D-PTV margin: No-, 2D-IG and organ registration using 3D-IG

$$\sum_{tot;3D} = \left(\sum_{intra-treat}{}^2 + \sum_{inter-treat}{}^2\right)^{1/2}$$
$$\sigma_{tot;3D}\left(\sigma_{intra-setup}{}^2 + \sigma_{intra-treat}{}^2 + \sigma_{inter-treat}{}^2\right)^{1/2} \quad (3)$$

Cumulative frequency distribution of CTV_{all} and PTV margins calculation

As described above, the uncertainties associated with CTV_{all} were calculated using the standard deviation of CTV_{all}. van Herk et al. described a PTV margin formula for minimal dose to 95% of the CTV in 90% of the patient population [6], in contrast, the cumulative frequency distributions of the actual CTV_{all} position were obtained to investigate the frequency tolerance level within 80,90,95 and 99% of CTV_{all}. The cumulative frequency distribution was approximated using polynomial regression ($R^2 > 0.99$) fitting.

For PTV generation, the CTV is generally expanded with a so-called "rolling ball" algorithm as a spherically symmetric condition [19]. As such, the prostate cancer CTV was considered an organ in the shape of an ellipsoid. Hence, to properly represent the 3D anisotropy of the CTV for a minimal dose prescription of 95% using the cumulative frequency distribution, the tolerance level must be more than 98.5% ; (i.e., the tolerance level was calculated using the formula (95% ≤ (x y z)), where x, y, and z, which correspond to LR, AP, and SI directions, respectively, were 98.5%. From this, the authors used a 99% tolerance level to compute the margin size in each direction for CTV_{all}.

To prescribe the minimum dose of the 95% the CTV for each vector of the PTV margin size ($M_{PTV:\,vector}$) for each IG procedure (no-IG, 2D-IG, and 3D-IG) was calculated using the RSS of Eq. (4) and the uncertainty components for each IG, shown in Table 1.

$$M_{PTV:vector} = \left(m_1{}^2 + m_2{}^2 + m_3{}^2 + m_4{}^2 + m_5{}^2\right)^{1/2}, \quad (4)$$

where m_1–m_5 were required to describe the margin size of the CTV position uncertainty, computed using cumulative frequency distributions of m_1: $CTV_{inter-setup}$; m_2: $CTV_{inter-organ}$; m_3: $CTV_{inter-treat}$; m_4: $CTV_{intra-setup}$;, and m_5: $CTV_{intra-treat}$ (Figure 1). The uncertainties with respect to the PTV margin for each IG procedure are listed in Table 1. To compare the margin size with our results, the no-IG, 2D-IG, and 3D-IG PTV margins were calculated using the margin formula of van Herk et al. ($M = 2.5\,\Sigma_{tot} + 0.7\,\sigma_{tot}$) [6].

Design of the equation to calculate the anisotropic PTV margins for H-IGRT

The anisotropic PTV margins can be calculated using the formula $M_{PTV:\,vector} = \alpha\,\Sigma_{tot} + \beta\,\sigma_{tot}$. $M_{PTV:\,vector}$ was calculated at a 99% confidence level based on the cumulative frequency distribution of CTV position error covering more than 95% of the dose distribution for the 3D margin (AP, SI, and LR). Σ_{tot} and σ_{tot}, the percentage of the CTV_{all} error, and the anisotropy of the PTV margin are given in Tables 3-5, respectively. The formula coefficients α and β for the PTV margin calculation ($M_{PTV:vector} = \alpha\,\Sigma_{tot} + \beta\,\sigma_{tot}$) were estimated using a least-squares matrix operation.

IRB

The study design was approved by our institutional review board.

Results

Systematic (Σ) and random (σ) uncertainties of CTV_{all}

The systematic (Σ) and random (σ) uncertainties of CTV for each IG condition are shown in Figure 1. The uncertainty components of the CTV position error with respect to the PTV margin are shown in Table 1. Σ, σ, and the mean of these uncertainty components are listed in Table 2; the values for Σ and σ are represented as Gaussian distributions. The uncertainty of the CTV position for each IG procedure increased in the order AP, SI, and LR for both Σ and σ. According to van Herk et al., Σ for each dimension was larger than σ [6], similar to our results, with Σ having a greater value than σ overall (Table 2).

Σ_{tot} and σ_{tot} values for each IG were computed using Eqs. (1) – (3). For the H-IGRT strategy proposed in this study, systematic and random errors were revised progressively over the IG procedure (no-IG, 2D-IG, and 3D-IG); hence, Σ_{tot} and σ_{tot} were relatively small after the completion of 3D-IG (Table 3).

Although Σ_{tot} and σ_{tot} for the SI and LR directions for 2D-IG and 3D-IG showed the same results, the individual uncertainty components differed, as shown in Table 1. As described above, the authors adopted

Image-guided strategy	Systematic (Σ_{tot}) (mm)			Random (σ_{tot}) (mm)		
	AP	SI	LR	AP	SI	LR
No-IG	3.0	1.7	1.6	1.2	1.0	0.6
2D-IG	2.2	1.2	0.4	1.0	0.9	0.4
3D-IG	1.4	1.2	0.5	1.0	0.9	0.4
The systematic (Σ_{tot}) and random (σ_{tot}) uncertainties represent the combined uncertainties shown in Table 2. No-IG: skin mark setup, no correction; 2D-IG: skin mark setup combined with bone registration using bone anatomy; 3D-IG: No-IG and 2D-IG procedures combined, with preferential organ registration to the anterior rectal wall.						

Table 3: Systematic (Σ_{tot}) and random (σ_{tot}) overall uncertainties in each image guidance procedure.

Percentage of the CTV position within tolerance	$CTV_{inter\text{-}setup}$; m_1 (mm)			$CTV_{inter\text{-}organ}$; m_2 (mm)			$CTV_{inter\text{-}treat}$; m_3 (mm)			$CTV_{intra\text{-}setup}$; m_4 (mm)			$CTV_{intra\text{-}treat}$; m_5 (mm)		
	AP	SI	LR	AP	SI	LR	AP	SI	LR	AP	SI	LR	AP	SI	LR
80%	4.5	1.5	3.5	3.5	1.5	1.5	2.8	0.6	1.9	3.0	1.0	1.3	1.4	0.3	0.3
90%	5.8	2.5	4.0	4.8	2.1	1.9	3.8	2.0	2.0	3.6	2.0	1.8	2.3	0.6	0.6
95%	7.0	2.7	4.5	5.4	3.6	2.1	4.4	2.5	2.3	4.0	3.5	2.1	3.0	1.2	0.9
99%	9.5	2.8	4.8	6.0	5.0	2.3	5.0	3.0	2.5	4.1	4.0	2.2	4.0	2.0	1.2
Here, m_1–m_5 represents the margin size required for each uncertainty component of the CTV. The percentage of the CTV position error within tolerance levels was calculated using polynomial regression fitting of the cumulative frequency distribution curve shown in Figure 3.															

Table 4: Percentage of the CTV_{all} position error and tolerance level of the uncertainty components.

the anterior rectal wall registration for the 3D-IG procedure. Therefore, despite prior rectal preparation, rectal filling had an impact on CTV position in 3D-IG; specifically, the LR value was greater than that for 2D-IG.

Comparison of the PTV margin sizes using the theoretical formula and actual distributions of the variations in CTV position in our H-IGRT strategy

The cumulative dose frequency distributions of CTV position errors were obtained using inter- and intra-fractional error for CTV_{all}. The curves of the cumulative dose frequency distributions were computed using polynomial regression ($R^2 > 0.99$) fitting (Figure 3).

The approximate expressions shown in Figure 3 were then used to compute the PTV margin size within tolerance levels of 80, 90, 95 and 99% for the five components (Table 5). Among the individual components, $CTV_{inter\text{-}setup}$ had the greatest influence on PTV margin size, followed by $CTV_{inter\text{-}organ}$, $CTV_{inter\text{-}treat}$, $CTV_{intra\text{-}setup}$, and $CTV_{intra\text{-}treat}$ (Table 4). Intra-fractional organ motion and intra-fractional setup uncertainty values ($CTV_{intra\text{-}setup}$ and $CTV_{intra\text{-}treat}$) were similar to others in the literature [20,21]. The maximum position error of the CTV was in the AP direction of $CTV_{inter\text{-}setup}$ (>9.0 mm, 99% confidence level).

The PTV margins (No-PTV margin, 2D-PTV margin and 3D-PTV margin) were computed using the RSS of the uncertainties of CTV under each IG condition (Tables 1 and 5). The margin sizes corresponding to a 99% tolerance level for a prescription dose of 95% for the anisotropic margin size of CTV are listed in Table 5.

The 3D-PTV margin size required for the H-IGRT was 7.6, 5.4, and 3.5 mm in the AP, SI, and LR directions, respectively. Comparing our results for the PTV margin size with those obtained using van Herk's formulation ($M_{PTV} = 2.5\,\Sigma_{tot} + 0.7\,\sigma_{tot}$), our PTV margin was larger in all three directions (Table 6). The maximum difference observed for each IG was as follows: no-IG: 4.3 mm (AP); 2D-IG: 3.0 mm (SI); and 3D-IG: 3.3 mm (AP). Using van Herk's formula, both the 2D- and 3D-PTV margins in the LR direction were 1.3 mm; these sizes are not suitable for clinical use.

Design of an anisotropic PTV margin for H-IGRT

In this study, α and β in the equation ($M_{PTV} = \alpha\,\Sigma_{tot} + \beta\,\sigma_{tot}$) were derived for the calculation of the anisotropic PTV margin via H-IGRT.

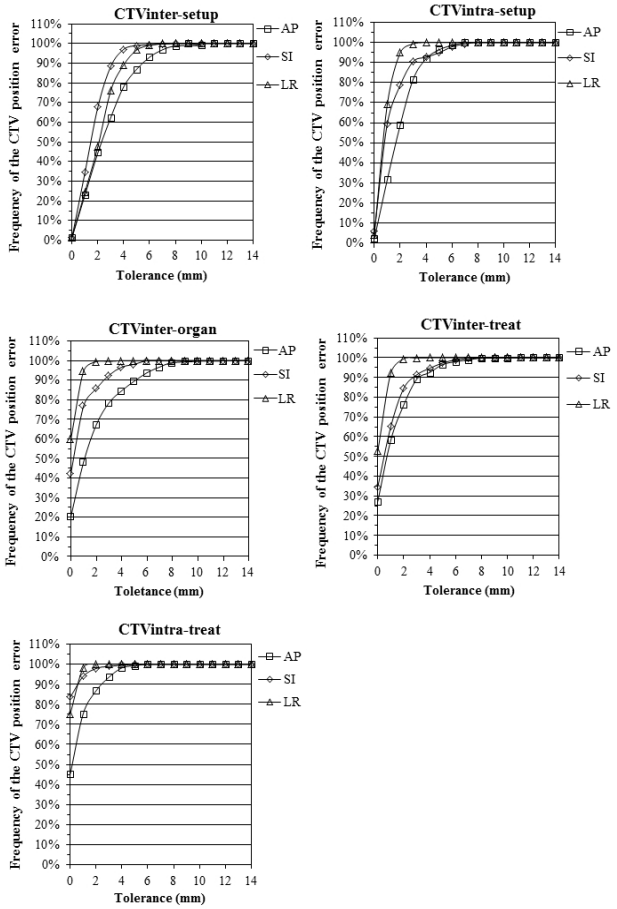

Figure 3: Cumulative frequency distributions of CTV_{all} position error are represented as cumulative frequency distributions of the inter- and intra-fractional uncertainties of CTV_{all}. CTV_{all} consisted of $CTV_{inter\text{-}setup}$, $CTV_{intra\text{-}setup}$, $CTV_{inter\text{-}treat}$, $CTV_{intra\text{-}treat}$, and $CTV_{inter\text{-}organ}$. The tolerance levels of the inter- and intra-fractional variations of CTV_{all} (the five uncertainty components) were calculated using polynomial regression ($R^2 > 0.99$) of the cumulative frequency distributions to each vector of the five uncertainty components.

Σ_{tot} and σ_{tot} were obtained from the uncertainties for CTV_{all}, shown in Table 3. M_{PTV} for a prescription dose of 95% to the CTV was determined using the cumulative frequency distributions of CTV_{all} shown in Table 6. Accordingly, α and β in this equation were computed using a least squares matrix operations (Table 7). Σ_{tot} and σ_{tot} were reduced during the H-IGRT procedure (Figure 1) due to the progressive corrections that occurred for each process (no-IG, 2D-IG, and 3D-IG). Consequently, for adequate anisotropic PTV margin size calculations, α ranged from 2.3–5.5 and β was 2.8–3.0 (Table 7).

Discussion

The authors performed online correction using H-IGRT to all fractions for prostate cancer patients undergoing VMAT. The H-IGRT strategy corrected for the systematic and random errors of CTV. The systematic (Σ_{tot}) and random uncertainties (σ_{tot}), according to the each IG correction protocol were computed with image data sets acquired for inter- and intra-fractional errors of CTV (Tables 1 and 2). Additionally, the proposed PTV margin calculation considered not only inter-fractional prostate movement which was acquired from each IGRT procedure but also a TRE that arise with No-, 2D- and 3D-IG.

CTV position exhibits anisotropic variation; thus, the PTV margin size calculation must consider all three dimensions for a minimum dose of more than 95% to the CTV. The CTV is generally expanded with a "rolling ball" algorithm [19] as a spherically symmetric condition in treatment planning for prostate cancer. In this instance, each PTV margin direction should be kept within 98.5% tolerance for a minimum dose of >95% to the CTV. Using the proposed H-IGRT strategy, the 3D-PTV margin size was 7.6, 5.4, and 3.5 mm in the AP, SI, and LR directions, respectively (Table 5), whereas the current PTV margin in the current study (8.0 mm in all dimensions, except posteriorly, where it was 5.0 mm) were barely reduced. Since the authors are adopting anterior rectal wall registration, rectal side margin will be enough at 5.0 mm.

With regard to daily variations in prostate position, several authors described prostate movement of 6.0–20.0 mm in each direction by inter-fractional organ motion or deformation [22-24]; inter-fractional organ motions are larger than intra-fractional motions [25]. Thus, without online IGRT procedures, safety margins of 10.0 mm for the AP and SI directions and 8.0 mm in the LR direction around the prostate have been recommended [1,2]. Hurkmans et al. and Rudat et al. [1,2] computed the PTV margin from actual inter-fractional setup uncertainty; safety margins of 8.0 mm (LR) and 10.0 mm (AP and SI) were reported for prostate cancer patients. Smitsman et al. and Meijer et al. [17,26] considered inter-fractional organ motion uncertainty and residual error of the seminal vesicles in their margin design.

In the present study, the PTV margin size was calculated using the cumulative frequency distributions of inter- and intra-fractional variations and TRE, which included the seminal vesicles in the CTV. The margin of the no-IG (only skin mark setup) were 12.6, 7.3, and 5.9 mm for the AP, SI, and LR directions, respectively, calculated using the cumulative frequency distribution of CTV_{all}. Σ_{tot} and σ_{tot} were substituted into van Herk's et al. formula ($M = 2.5\ \Sigma_{tot} + 0.7\ \sigma_{tot}$), and the PTV margin was calculated again, revealing margins of 8.3, 5.0, and 4.4 mm for the AP, SI, and LR directions, respectively. The maximum difference between those results and ours was observed in the AP direction. Also, the 2D- and 3D-PTV margins using van Herk et al. were 1.7–3.4 mm smaller than our results (Table 6). Meijer et al. [26] computed the PTV margin size using a model-based deformable image registration and online IGRT, and compared their results with van Herk et al. [6], whose values were reportedly smaller by a maximum of 3.0, 2.0, and 2.0 mm in the AP, SI, and LR directions, respectively. Coverage in each direction of the CTV computed using the margin size formula proposed by van Herk et al. was no more than 80–95%, with 3D coverage limited to 51–86% (Tables 5 and 6).

Engels et al. [27] analysed the correlation of the PTV margin size and impact on the five-year freedom from biochemical failure (FFBF) in IGRT for prostate cancer. The PTV margins of 5.0, 4.0, and 3.0 mm (AP, SI, and LR, respectively) were compared with an isotropic PTV margin of 6.0 mm in all directions; PTV margins of 6.0 mm in all directions indicated a five-year FFBF percentage of 96%, compared with 74% for the tighter PTV margin group. In our results, the PTV margin sizes with $M_{PTV}=2.5\ \Sigma_{tot}+0.7\ \sigma_{tot}$ were 4.2, 3.7 and 1.3 mm (in the AP, SI, and LR directions, respectively); thus, the PTV margin may be inadequate if van Herk et al.'s formula is used for H-IGRT. Given this margin size, the coverage would range from 51 to 86% for the 3D CTV. Hence, the authors concluded that the use of the $M_{PTV}=2.5\ \Sigma_{tot}+0.7\ \sigma_{tot}$ formula for prostate cancer may be inadequate.

Van Herk et al. assumed that organ movement could be represented by a normal probability distribution; the margin recipe was represented with one formula for all directions for the PTV calculation. In contrast, our recipe offers greater flexibility in that it can accommodate random variation using a cumulative distribution function, because uncertainty of CTV position of the respective direction has a certain variance and distribution. Additionally, H-IGRT can cover variations in the CTV position for each vector, using our recipe, by correcting for nearly all associated systematic errors. More specifically, assuming that Σ is zero by use of the H-IGRT system, and then the calculation for the PTV margin size considers only the random uncertainty (σ), which is simply multiplied by a coefficient value, ranges from 2.8–3.0 to the σ. In this study, the proposed method considers equations for the PTV margin calculation for No, 2D and 3D-IGRT in three axes, AP, SI, and LR.

Conclusion

H-IGRT was corrected for systematic and random errors of the CTV for almost all fractions. The margin size (M_{PTV}) was calculated

Percentage of the CTV position within tolerance	No-PTV margin (mm)			2D-PTV margin (mm)			3D-PTV margin (mm)		
	AP	SI	LR	AP	SI	LR	AP	SI	LR
80%	6.6	2.4	4.0	4.8	1.8	2.0	4.3	1.2	2.3
90%	8.7	3.9	4.8	6.4	3.0	2.7	5.7	2.9	2.8
95%	10.2	5.8	5.5	7.4	5.2	3.1	6.7	4.5	3.2
99%	12.6	7.3	5.9	8.3	6.7	3.4	7.6	5.4	3.5
No-IG, 2D-IG, and 3D-IG PTV margins. The anisotropy of the PTV margin size was calculated using the root sum square (RSS) of the uncertainty components (Table 4) necessary for the PTV margin design. $M_{PTV:vector} = (m_1^2 + m_2^2 + m_3^2 + m_4^2 + m_5^2)^{1/2}$. $M_{PTV:vector}$ is the margin size in each direction. m_1–m_5 are listed in Table 4.									

Table 5: Anisotropy of the PTV margin size computed using the frequency distributions of the CTV position variation.

PTV of image-guided strategy	PTV margin size (mm)					
	AP		SI		LR	
	*van Herk et al.	† Present study	*van Herk et al.	† Present study	*van Herk et al.	† Present study
no-PTV margin	8.3	12.6	5.0	7.3	4.4	5.9
2D-PTV margin	6.3	8.3	3.7	6.7	1.3	3.4
3D-PTV margin	4.2	7.6	3.7	5.4	1.3	3.5
No-, 2D-, and 3D-PTV margins are the necessary margin size from each IG procedure. *Each PTV margin was calculated using the equation of MPTV = 2.5 Σ_{tot}+0.7 σ_{tot} reported by van Herk et al. [6] for the PTV margin from statistical considerations. † The PTV margin size was calculated with respect to 95% dose coverage to the CTV based on the polynomial regression fitting of the cumulative frequency distribution curve (R^2 > 0.99).						

Table 6: Comparison of the PTV margin size using the formula given by van Herk et al. (M_{PTV} = 2.5 Σ_{tot} + 0.7 σ_{tot}) and the actual distributions of the CTV position using the proposed H-IGRT strategy.

	No-PTV margin		2D-PTV margin		3D-PTV margin	
	α	β	α	β	α	β
AP	3.0	3.0	2.5	2.8	3.4	2.9
SI	2.6	2.9	3.4	3.0	2.3	3.0
LR	2.6	2.9	5.5	3.0	4.6	3.0
No-, 2D-, and 3D-PTV margins represent the necessary margin size for each IG.						

Table 7: Estimate of α and β coefficients from the formula ($M_{PTV: vector}$ = αΣ + βα) for the PTV margin size computation.

using a novel formula that accounted for the anisotropy of the organ considered (the prostate); the recipe satisfied a 99% prescription dose in three directions (AP, SI, and LR). Moreover, using the H-IGRT procedure, the minimum dose to the CTV was 95% of the prescribed dose over three dimensions for all prostate cancer patients.

Acknowledgment

The authors would like to thank their colleagues for their support in the data analysis.

Funding

This study was supported in part by a Grant-in-Aid for Cancer Research (H26-090) from the Ministry of Health, Labour and Welfare of Japan, and by the National Cancer Centre Research and Development Fund (26-A-4).

References

1. Hurkmans CW, Remeijer P, Lebesque JV, Mijnheer BJ (2001) Set-up verification using portal imaging; review of current clinical practice. Radiother Oncol 58: 105-120.
2. Rudat V, Flentje M, Oetzel D, Menke M, Schlegel W, et al. (1994) Influence of the positioning error on 3D conformal dose distributions during fractionated radiotherapy. Radiother Oncol 33: 56-63.
3. de Crevoisier R, Tucker SL, Dong L, Mohan R, Cheung R, et al. (2005) Increased risk of biochemical and local failure in patients with distended rectum on the planning CT for prostate cancer radiotherapy. Int J Radiat Oncol Biol Phys 62: 965-973.
4. Wong JR, Grimm L, Uematsu M, Oren R, Cheng CW, et al. (2005) Image-guided radiotherapy for prostate cancer by CT-linear accelerator combination: prostate movements and dosimetric considerations. Int J Radiat Oncol Biol Phys 61: 561-569.
5. Ghilezan M, Yan D, Liang J, Jaffray D, Wong J, et al. (2004) Online image-guided intensity-modulated radiotherapy for prostate cancer: How much improvement can we expect? A theoretical assessment of clinical benefits and potential dose escalation by improving precision and accuracy of radiation delivery. Int J Radiat Oncol Biol Phys 60: 1602-1610.
6. van Herk M, Remeijer P, Rasch C, Lebesque JV (2000) The probability of correct target dosage: dose-population histograms for deriving treatment margins in radiotherapy. Int J Radiat Oncol Biol Phys 47: 1121-1135.
7. Gay HA, Barthold HJ, O'Meara E, Bosch WR, El Naqa I, et al. (2012) Pelvic normal tissue contouring guidelines for radiation therapy: a Radiation Therapy Oncology Group consensus panel atlas. Int J Radiat Oncol Biol Phys 83: e353-362.
8. Suzuki M, Nishimura Y, Nakamatsu K, Okumura M, Hashiba H, et al. (2006) Analysis of interfractional set-up errors and intrafractional organ motions during IMRT for head and neck tumors to define an appropriate planning target volume (PTV)- and planning organs at risk volume (PRV)-margins. Radiother Oncol 78: 283-290.
9. Suzuki M, Nakamatsu K, Kanamori S, Okumra M, Uchiyama T, et al. (2003) Feasibility study of the simultaneous integrated boost (SIB) method for malignant gliomas using intensity-modulated radiotherapy (IMRT). Jpn J Clin Oncol 33: 271-277.
10. Jin JY, Yin FF, Tenn SE, Medin PM, Solberg TD (2008) Use of the BrainLAB ExacTrac X-Ray 6D system in image-guided radiotherapy. Med Dosim 33: 124-134.
11. Mayyas E, Chetty IJ, Chetvertkov M, Wen N, Neicu T, et al. (2013) Evaluation of multiple image-based modalities for image-guided radiation therapy (IGRT) of prostate carcinoma: a prospective study. Med Phys 40: 041707.
12. Dogan N, Song S, Saleh H, Wu J, Murphy MJ (2010) Comparisons of multiple automated anatomy-based image-guidance methods for patient setup before head/neck external beam radiotherapy. J Appl Clin Med Phys 12: 3337.
13. Wong JR, Gao Z, Uematsu M, Merrick S, Machernis NP, et al. (2008) Interfractional prostate shifts: review of 1870 computed tomography (CT) scans obtained during image-guided radiotherapy using CT-on-rails for the treatment of prostate cancer. Int J Radiat Oncol Biol Phys 72: 1396-1401.
14. Schallenkamp JM, Herman MG, Kruse JJ, Pisansky TM (2005) Prostate position relative to pelvic bony anatomy based on intraprostatic gold markers and electronic portal imaging. Int J Radiat Oncol Biol Phys 63: 800-811.
15. Huang E, Dong L, Chandra A, Kuban DA, Rosen II, et al. (2002) Intrafraction prostate motion during IMRT for prostate cancer. Int J Radiat Oncol Biol Phys 53: 261-268.
16. Boda-Heggemann J, Köhler FM, Küpper B, Wolff D, Wertz H, et al. (2008) Accuracy of ultrasound-based (BAT) prostate-repositioning: a three-dimensional on-line fiducial-based assessment with cone-beam computed tomography. Int J Radiat Oncol Biol Phys 70: 1247-1255.
17. Smitsmans MH, de Bois J, Sonke JJ, Catton CN, Jaffray DA, et al. (2011) Residual seminal vesicle displacement in marker-based image-guided radiotherapy for prostate cancer and the impact on margin design. Int J Radiat Oncol Biol Phys 80: 590-596.
18. ICRU (1999) International Commission in Radiation Units and Measurements, "Prescribing, recording, and reporting photon beam therapy Report-62.
19. Remeijer P, Rasch C, Lebesque JV, van Herk M (2002) Margins for translational and rotational uncertainties: a probability-based approach. Int J Radiat Oncol Biol Phys 53: 464-474.
20. Mah D, Freedman G, Milestone B, Hanlon A, Palacio E, et al. (2002) Measurement of intrafractional prostate motion using magnetic resonance imaging. Int J Radiat Oncol Biol Phys 54: 568-575.
21. Xie Y, Djajaputra D, King CR, Hossain S, Ma L, et al. (2008) Intrafractional motion of the prostate during hypofractionated radiotherapy. Int J Radiat Oncol Biol Phys 72: 236-246.

22. Graf R, Boehmer D, Budach V, Wust P (2012) Interfraction rotation of the prostate as evaluated by kilovoltage X-ray fiducial marker imaging in intensity-modulated radiotherapy of localized prostate cancer. Med Dosim 37: 396-400.

23. Ghilezan MJ, Jaffray DA, Siewerdsen JH, Van Herk M, Shetty A, et al. (2005) Prostate gland motion assessed with cine-magnetic resonance imaging (cine-MRI). Int J Radiat Oncol Biol Phys 62: 406-417.

24. Nichol AM, Brock KK, Lockwood GA, Moseley DJ, Rosewall T, et al. (2007) A magnetic resonance imaging study of prostate deformation relative to implanted gold fiducial markers. Int J Radiat Oncol Biol Phys 67: 48-56.

25. Balter JM, Sandler HM, Lam K, Bree RL, Lichter AS, et al. (1995) Measurement of prostate movement over the course of routine radiotherapy using implanted markers. Int J Radiat Oncol Biol Phys 31: 113-118.

26. Meijer GJ, de Klerk J, Bzdusek K, van den Berg HA, Janssen R, et al. (2008) What CTV-to-PTV margins should be applied for prostate irradiation? Four-dimensional quantitative assessment using model-based deformable image registration techniques. Int J Radiat Oncol Biol Phys 72: 1416-1425.

27. Engels B, Soete G, Gevaert T, Storme G, Michielsen D, et al. (2014) Impact of planning target volume margins and rectal distention on biochemical failure in image-guided radiotherapy of prostate cancer. Radiother Oncol 111: 106-109.